 FDMP, vol.2, no.1, pp.47-58, 2006

# Reconstruction of Interfaces between Electrically Conducting Fluids from Electrical Potential Measurements

**A.Kurenkov[1], A.Thess[2], and H.Babovsky[3]**

**Abstract:** A possibility for the determination of the interface between two electrically conducting fluids in cylindrical geometry is presented. The fluids with different conductivities are situated in an infinite cylinder. Along the axis of the cylinder a homogeneous electrical current is applied. The perturbation of the interface leads to an inhomogeneous electrical current and, therefore, results in an electrical potential change in the fluids and a magnetic field modification outside the fluids. The dependence of the electrical potential on the interface shape is obtained analytically. The interface profile is then recovered from data of the electrical potential measurements which have been generated numerically. This inverse problem is solved for the cases of an axisymmetric and non-axisymmetric interface using the singular value decomposition method and Fourier transform. The number of modes which have to be reconstructed is obtained using L-curve criterion.

**keyword:** Electrical impedance tomography, Materials processing, Inverse boundary value problems, L-curve

## 1 Introduction

There are a variety of problems in materials processing where it would be useful to know the time-dependent distribution of the electrical conductivity of a single fluid or a multiphase flow. For instance, the knowledge of the position of the interface between highly conducting molten aluminium and poorly conducting liquid cryolite is important to prevent unwelcome instabilities in aluminium reduction cells Davidson (1999). Other examples include electrical conductivity distributions in glass melting furnaces, metal-slag interfaces in steel and ironmaking as well as on-line detection of inclusions Guthrie, Li, and Carrozza (2000). The liquids involved in materials processing such as molten metals, semiconductors, and glass melts are mostly hot and highly aggressive. Therefore conventional measurement techniques employing local probes face serious difficulties.

The purpose of the present work is to demonstrate that concepts of electrical impedance tomography (EIT) which have been successfully applied to a variety of medical problems Cheney, Isaacson, and Newell (1999) and multiphase flows George, Torczynski, Shollenberger, O'Hern, and Ceccio (2000), Butler and Bonnecaze (1999) can be used in order to locate interfaces between current carrying fluids of different electrical conductivity in high-temperature melts. The basic idea of our approach is to exploit to the greatest possible extent the electrical currents which are already present in materials processing operations such as aluminium reduction, electrical glass melting or vacuum arc remelting rather than to inject additional artificial electrical current as is usually done in EIT applications. In particular, we will demonstrate that the electrical current flowing through a highly simplified model of an aluminium reduction cell provides sufficient information to completely reconstruct the unknown position of the aluminium-cryolite interface.

For the reader it may be interesting to notice that the typical values of the interface displacement in the latter system are very small compared to the lateral extent of the system. Let us illustrate this by considering typical figures of a real aluminium reduction cell. Typically the cross-section of the aluminium reduction cell has a maximum length $L = 8m$. The applied electrical current is about $100kA$. The interface displacement $\eta$, the measurement of which is the main goal of our work, is of the order of several centimetres. It is well known from industrial practice that already such small interface displacement can perturb significantly the operation of an aluminium reduction cell. As a result, our problem is

[1] Department of Mechanical Engineering, Fluid Mechanics Group, Technical University of Darmstadt, 64287 Darmstadt, Petersenstrasse 13

[2] Department of Mechanical Engineering, Ilmenau University of Technology, P.O.Box 100565, 98684 Ilmenau, Germany

[3] Department of Mathematik, Ilmenau University of Technology, P.O.Box 100565, 98684 Ilmenau, Germany

characterised by a very small ratio $\varepsilon = \eta/L$ between the interface displacement and the lateral size of the system. Therefore we have decided to restrict the present analysis to $\varepsilon \ll 1$.

The statement of the considered problem is schematically shown in Fig. 1. Two fluids with different electrical conductivities $\sigma_1$ (upper) and $\sigma_2$ (lower) are situated in an infinite cylinder with the radius $R$. The cylinder walls are non-conducting. Along the axis of the cylinder a homogeneous electrical current with density $j_0$ is applied. If the interface between the fluids is flat, the electrical

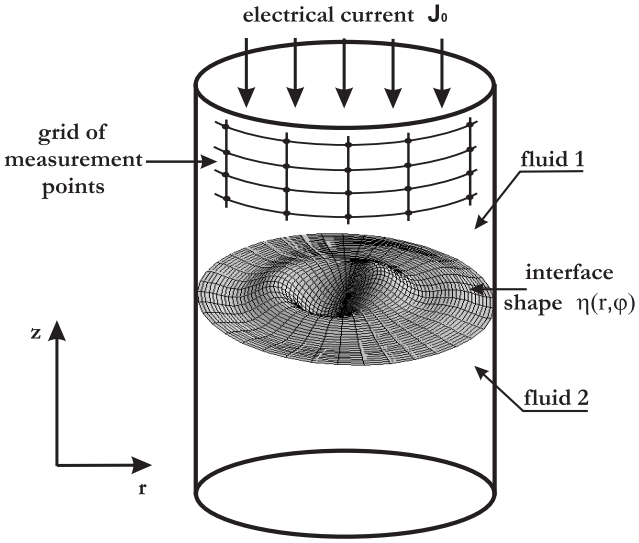


**Figure 1** : Statement of the problem.

current $\vec{J}$ is homogeneous everywhere (see Fig. 2 a). In this case the total electrical potential $\Phi$ is equal to the electrical potential $\Phi_0 = -j_0 z/\sigma$, induced by the applied electrical current $j_0$. As soon as the interface deviates from its flat shape due to interfacial waves or an external forcing, the electrical current density $\vec{J}$ will become nonhomogeneous near the interface (see Fig. 2 b). At $z \to \pm\infty$ the mean current $\vec{J}$ becomes asymptotically constant. The inhomogeneity of current $\vec{J}$ can be represented by the perturbation of electrical current density $\vec{j}$ (where $\vec{J} = \vec{j_0} + \vec{j}$) and it induces a perturbation of the electrical potential $\phi$ (where $\Phi = \Phi_0 + \phi$). The question as to whether we can reconstruct the interface shape from measurements of $\phi$ at the wall represents the central focus of our work.

It is also possible to reconstruct the interface from magnetic field, which is measured outside the cylinder. If the

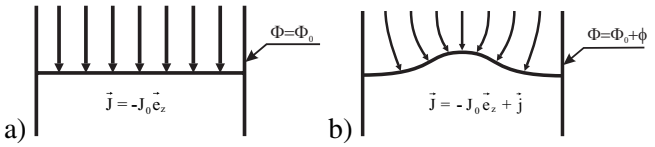


**Figure 2** : Non-homogeneity of electrical currents in case of interface perturbation. a) Flat interface, no current perturbation. b) Wrinkled interface, the current perturbation is presented.

perturbation of the fluid interface is non-axisymmetric, it leads to a perturbation of the magnetic field outside the cylinder. This fact can be used for interface reconstruction as well. But from the magnetic field measurements one can recover only non-axisymmetric interfaces, because an axisymmetric interface perturbation leads to the axisymmetric electrical current distribution and it does not induce a magnetic field perturbation outside the cylinder. This was the first reason, why we have chosen the reconstruction from the electric potentials. Another reason is, that the analysis with the electric potential amenable to analytical treatment in contrast to the magnetic problem. For these two reasons we consider in this paper only the problem of the interface reconstruction from the electrical potential measurements.

In our further discussion we will distinguish two tasks. The first task, the so-called forward problem, concerns the calculation of the electrical potential in the fluids from the interface perturbation. The second task, the so-called inverse problem, is devoted to the reconstruction of the interface shape from the electrical potential at the fluid-cylinder boundary. The solution of the forward problem is usually unique, i.e. one can obtain the electrical potential in the fluids from the interface perturbation data with high accuracy. The solution of the inverse problem is unstable in most cases. A small measurement error in the electrical potential data set induces a significant error in the reconstructed interface. Such problem is called ill-posed.

The present problem is similar in many respects to the tasks of electrical impedance tomography (EIT). EIT is a noninvasive technique for the construction of an approximation to the conductivity distribution in a given region from electrical potential data sets which are measured at the boundaries of the region Butler and Bonnecaze (1999). Directly at the boundaries of the considered region the testing electrical currents are applied.

This method is used in medicine for the detection of gas or blood location within the body. Cheney at al. Cheney, Isaacson, and Newell (1999) provide a detailed description of the medical application of EIT. There are also other applications of EIT. Butler at al. Butler and Bonnecaze (1999) have shown the possibility to determine particle migration for a pressure-driven tube flow with the help of EIT. In our work we shall use algorithms which are more simple than in traditional EIT applications. We have used only one testing electrical current with comparatively few measurement points.

The structure of the present paper is organised as follows. In the next section we describe the solution of the forward problem. The dependence of the electrical potential in the fluids on the interface perturbation is studied in detail. The algorithm for the reconstruction is presented in section 3. Examples of a complete interface shape reconstruction are demonstrated in section 4. In section 5 we summarise our conclusion and discuss some topics that would be useful to investigate in future.

## 2 Forward problem

### 2.1 The interface perturbation

We consider small deviations of the interface position $z = \eta(r,\varphi,t)$ from its unperturbed location in the plane at $z = 0$. More precisely, we shall assume that $\eta \ll R$. We will restrict our attention to a cylindrical geometry. However, the present analysis can be extended to infinite rods with arbitrary cross sections.

The interface displacement can be represented in the form Miles and Henderson (1990)

$$\eta(r,\varphi,t) = \sum_{i=1}^{\infty} \xi_i(t)\psi_i(r,\varphi) \tag{1}$$

where $\psi_i(r,\varphi)$ is a complete set of orthonormal functions satisfying Neumann boundary conditions $\partial\psi_i/\partial r$ at $r = R$. Using the Bessel functions as a basis we can write any interface displacement in the form

$$\eta(r,\varphi,t) = \sum_{m=-M}^{M}\sum_{n=1}^{N} c_{mn}(t)J_m(k_{mn}r)\,e^{im\varphi} \tag{2}$$

where $c_{mn}$ is the complex amplitude of the interface modes, $J_m$ is the Bessel function of the first kind, $k_{mn} = y_{mn}/R$ and $y_{mn}$ is the $n$-th solution of the equation $J'_m(r) = 0$. In the case $m = 0$ we omit the solution $y_{00} = 0$ because this solution corresponds to the flat surface $\eta(t) = const$. Here a limited number of modes $M$ and $N$ is used. It can be shown Dyachenko, Korotkevich, and Zakharov (2004), that the amplitudes of higher modes decline as $< |\eta_k|^2 > \sim k^{-7/2}$. The higher modes can be neglected.

Equation (2) describes the general case of a non-axisymmetric interface. For the axisymmetric case ($m = 0$) this equation simplifies to

$$\eta(r,t) = \sum_{n=1}^{N} c_n(t)J_0(k_n r) \tag{3}$$

If the interface undergoes free oscillations, the time-dependent coefficients in equations (2) and (3) have the form $c_{mn}e^{i\omega t}$. The oscillation frequency $\omega$ can be obtained from linear stability analysis. It should however be noted that we do not consider the dynamical origin of the time-dependent amplitudes $c_{mn}(t)$ since the subsequent theory depends only on their instantaneous values.

### 2.2 Electrical potentials in the fluids

The interface perturbation $\eta$ leads to an inhomogeneous distribution of the total electrical current density $\vec{J}$ in the fluids. This inhomogeneous current density can be written as

$$\vec{J} = -j_0\vec{e}_z + \vec{j} \tag{4}$$

where $j_0$ is the density of the mean electrical current and $\vec{j}$ the perturbation of the current density. The present analysis is valid for both direct current and low-frequency alternating electrical current where the skin effect can be neglected. The maximal allowable frequency of the electrical current can be estimated by $\delta \ll R$, where $\delta$ is the skin depth. In our case this leads to the requirement that the frequency $f$ of the alternating current is limited as

$$f \ll \frac{1}{2\pi\mu_0\sigma R^2}$$

where $\sigma$ is the electrical conductivity of the fluid with the higher conductivity. The total electrical potential in the fluid is then

$$\Phi = \Phi_0 + \phi \tag{5}$$

where $\phi$ is the perturbation of the electrical potential which is induced by the perturbation of the current density $\vec{j}$. The perturbations of the electrical current $\vec{j}$ and

the electrical potential $\phi$ are caused by the interface perturbation $\eta(r,\varphi)$. If the interface $\eta(r,\varphi)$ is flat, then $\vec{j}=0$ and $\phi=0$. $\Phi_0$ is induced by the homogeneous electrical current density $j_0$. The solution for $\Phi_0$, called the basic solution, follows from the Ohms law with boundary condition $\Phi_0=0$ for $z=0$:

$$\Phi_0=\frac{j_0 z}{\sigma} \tag{6}$$

Perturbation of electrical potential $\phi$ satisfies

$$\triangle\phi_1=\triangle\phi_2=0 \tag{7}$$

with the system of the four boundary conditions

$$\frac{\partial\phi}{\partial r}=0, \qquad \text{for } r=R \tag{8}$$

$$\phi_1=\phi_2=0, \qquad \text{for } z=\pm\infty \tag{9}$$

$$\phi_1-\phi_2=j_0\eta\left[\frac{1}{\sigma_2}-\frac{1}{\sigma_1}\right], \qquad \text{for } z=0 \tag{10}$$

$$\sigma_1\frac{\partial\phi_1}{\partial z}=\sigma_2\frac{\partial\phi_2}{\partial z}, \qquad \text{for } z=0 \tag{11}$$

The first condition (8) expresses the fact of the non-conductivity of the cylinder walls and the second condition (9) expresses the vanishing of the electrical potential perturbation for $z=\pm\infty$. The last two conditions (10)-(11) follow from the continuity of the tangential component of the electrical field and the normal component of the electrical current density respectively at the interface. The exact conditions are $\vec{J}_1\cdot\vec{n}=\vec{J}_2\cdot\vec{n}$ and $\Phi_1=\Phi_2$ along the interface $z=\eta(r,\varphi)$. These two conditions were linearised around $z=0$ so as to solve the problem analytically. This method which is based on the assumption of small interface perturbation was commonly used for the analysis of aluminium reduction cells (see e.g. DavidsonDavidson (1994)).

The harmonic function which satisfies all four boundary conditions is determined from the ansatz Davidson (1994)

$$\phi_i(r,\varphi,z)=\frac{j_0\eta(r,\varphi)}{\sigma_i}f_i(z), \tag{12}$$

where $\sigma_i$, $i=1,2$ is the conductivity in the corresponding fluid. Subscript 1 denotes the first one and subscript 2 the second one respectively. $f_i(z)$ are the some functions which have to be determined, $j_0$ is the density of the mean electrical current, $\eta(r,\varphi)=c_{mn}J_m(k_{mn}r)e^{im\varphi}$ is the interface. This expression is valid for both fluids. Condition (8) is automatically satisfied because the first derivative of $\eta(r,\varphi)$ vanishes at $r=R$. Substituting the expression (12) in equation (7) and using the condition (9) we obtain $f_1(z)=b_1\cdot\exp(-k_{mn}z)$ and $f_2(z)=b_2\cdot\exp(k_{mn}z)$. We find the constants $b_1$ and $b_2$ from the boundary conditions (10)-(11) as $b_1=-b_2=(\sigma_1-\sigma_2)/(\sigma_1+\sigma_2)$. The electrical potential perturbation in the fluid is the superposition of the elementary potential perturbations caused by each single mode of the interface perturbation. The total potential perturbation in the fluids satisfies

$$\phi_i(r,\varphi,z) = sign[z]\frac{j_0}{\sigma_i}\frac{\sigma_1-\sigma_2}{\sigma_1+\sigma_2}\sum_{m=-M}^{M}\sum_{n=1}^{N}c_{mn}J_m(k_{mn}r)\,e^{im\varphi-k_{mn}|z|} \tag{13}$$

For the axisymmetric interface case $(m=0)$ this expression simplifies to

$$\phi_i(r,z)=sign[z]\frac{j_0}{\sigma_i}\frac{\sigma_1-\sigma_2}{\sigma_1+\sigma_2}\sum_{n=1}^{N}c_nJ_0(k_nr)\,e^{-k_n|z|} \tag{14}$$

The perturbations of the electrical potential $\phi$ in the fluid at the cylinder boundary caused by a single mode of the interface perturbation $\eta(r,\varphi)$ are shown in Fig. 3. The perturbations appear in both fluids, but they are higher in the poorly conducting fluid.

For large interface displacements the boundary conditions at the interface $z=\eta$ can not be linearised anymore and the forward problem would have to be solved numerically. However, such fully numerical solution does not provide a clear understanding of the dependence of the electrical potential perturbation $\phi$ on the interface displacement $\eta$. By contrast, the analytical solution gives a comparatively simple expression which makes a qualitative analysis of the last dependence possible. Therefore we use in the following parts of this paper only the analytical solution of the forward problem.

### *2.3 Non-dimensional equations*

We define the dimensionless variables $r^*,z^*,\eta^*,\phi^*$ by $z^*=z/R$, $r^*=r/R$, $\eta^*=\eta/R$, $\phi_i^*=\phi_i\sigma_i/j_0R$. In the dimensionless equations the expressions $k_{mn}r$ will be transformed to $y_{mn}r^*$. The dimensionless equation for the electrical potential in the non-axisymmetric case is thus

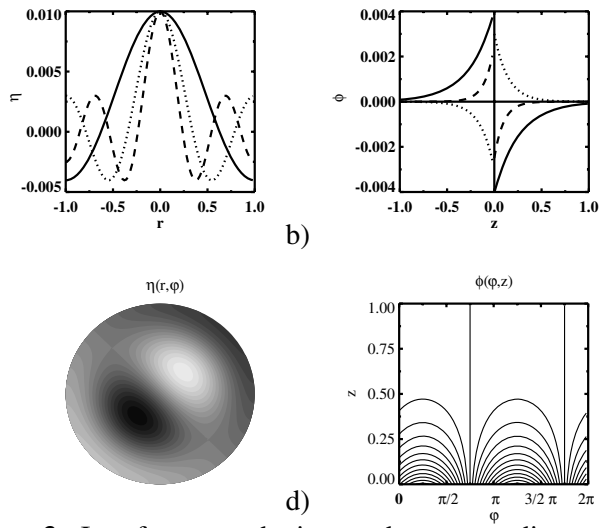


**Figure 3** : Interface perturbations and corresponding potential perturbations: in Figure a) the axisymmetric interface for the first, second and third radial modes (the modes (0,1), (0,2), (0,3)) is shown. Figure b) presents the dependence of the potential perturbation $\phi$ on $z$ in the fluid at the cylinder boundary, where $\phi$ is caused by a single mode of the axisymmetric interface perturbation $\eta(r)$. The —— represents the potential perturbation which is obtained for the first radial mode of interface perturbation, the $\cdots\cdots$ for the second radial mode, the - - - - for the third radial mode. In Figure c) the non-axisymmetric interface [the mode (1,2)] is shown and in Figure d) the caused by its potential perturbation at the fluid boundary is presented.

modified to

$$\phi_i(r,\varphi,z) = sign[z] \sum_{m=-M}^{M} \sum_{n=1}^{N} c_{mn} J_m(y_{mn} r)\, e^{im\varphi - y_{mn}|z|} \quad (15)$$

and in the axisymmetric case it is transformed to

$$\phi_i(r,z) = sign[z] \sum_{n=1}^{N} c_n J_0(y_n r)\, e^{-y_n|z|} \quad (16)$$

In the remaining part of paper we will use only non-dimensional variables. Evaluating equations (15) and (16) at the cylinder wall $r = 1$ we finally arrive at the equations providing the link between the surface deflection (described by the expansion coefficients $c_{mn}$ or $c_n$) and the potential distribution at the walls. These equations form the mathematical basis of our work. The rest of the paper is devoted to the treatment of the inverse problem $\phi(\varphi,z) \rightarrow c_{mn}$ or $\phi(z) \rightarrow c_n$.

It must be remarked, that for the reconstruction of the interface it is sufficient to have the data set of the electrical potentials at the fluid boundary in one of the fluids only. Therefore we consider only one fluid further in this paper. The $sign[z]$ will be taken positive in the equations describing the dependence of the electrical potential perturbation on the interface perturbation. The computation of the position of the unperturbed interface ($\eta = 0$) is not the aim of this paper, but some possibilities will be be discussed in the subsection 3.1.

### *2.4 The error in potential resulted from truncated form of representation*

We represent the electrical potential perturbation resulted from the interface deflection in the form given by eq. 16. This equation contains a finite numer of modes (number $N$ in eq. 16). In the reality we can have a more complicated case with a infinite number of modes ($N = \infty$). The difference between the real case with infinite number of modes ($N = \infty$) and truncated representation ($N = const$) forms the model error

$$e_k = \sum_{N+1}^{\infty} c_n J_0(y_n) e^{-y_n z_k}. \quad (17)$$

which we will discuss here. In principle the model error can be defined for both fluids, for the case of simplicity we assume to be $0 < z < \infty$.

Dyachenko *et al.* Dyachenko, Korotkevich, and Zakharov (2004) have been shown that the amplitudes of interfacial waves decreases as

$$< |c_n| > \sim y^{-7/4} \quad (18)$$

where n is the mode number. Based on this, the expression (17) is simplified to

$$e_k \leq \sum_{N+1}^{\infty} y_n^{-7/4} J_0(y_n). \quad (19)$$

We note, that $0 < z < \infty$ and, therefore, $e^{-y_n z_k} < 1$.

This infinite sum can be estimated with help of geometrical regression. The quotient of two neighboring elements with $m \geq N+1$ is

$$q = a_{m+1}/a_m = \left(\frac{y_m}{y_m+1}\right)^{7/4} \frac{J_0(y_{m+1})}{J_0(y_m)} < 1 \quad (20)$$

The first term of the geometrical regression is

$$a_0 = y_{N+1}^{-7/4} J_0(y_{N+1}) \quad (21)$$

Using the formula for the sum of the geometrical regression

$$R_n = \frac{a_0}{1-q}, \tag{22}$$

we obtain:

$$e_n = R_n \leq \frac{y_{N+1}^{-7/4} J_0(y_{N+1})}{1 - \left(\frac{y_{N+1}}{y_{N+2}}\right)^{(7/4)} \frac{J_0(y_{N+1})}{J_0(y_{N+2})}} \tag{23}$$

The last expression shows, that the electrical potential can be computed form a know interface with any given accuracy which only depends on the number of modes included in interface representation. The more modes included the better the potential perturbation is computed. So, we can operate with a small number of first modes and we neglect the higher modes without a significant lost of accuracy.

## 3 Inverse problem

### 3.1 Basic location of the interface

For the following interface reconstruction we need to known the position of the basic flat interface. For an experiment or application a cylinder of large but finite height $H$ could be used, in which the mean electrical current $\vec{J}$ could be applied between electrodes. Therefore in this subsection we consider the determination of the basic location for a finite cylinder.

If the interface is non-disturbed, the basic interface location can be easily determined from the measurements of the mean electrical current density $j_0$ and from the voltage $U$ between two electrodes. The conductivities of the fluids $\sigma_1$ and $\sigma_2$ and the height of the cylinder $H$ are also known. To find the interface position, we need to evaluate the expression for the mean electrical current. The last could be computed from the Ohms law as

$$j_0 = U \frac{\sigma_1 \sigma_2}{\sigma_2 h_1 + \sigma_1 h_2} \tag{24}$$

where $h_1$ is the distance between interface and lower electrode, $h_2$ between interface and upper electrode. Substituting $h_1 = H - h_2$ in the last equation, we obtain

$$h_2 = \frac{U}{j_0} \frac{\sigma_1 \sigma_2}{\sigma_1 - \sigma_2} - \frac{\sigma_2}{\sigma_1 - \sigma_2} H \tag{25}$$

In the practice in the aluminium reduction cells the current density and the voltage between electrodes are measured automatically, so that the location of basic interface presents no difficulty.

If the interface undergoes small oscillations, the electrical voltage $U$ becomes also oscillating near the value, which corresponds to the case without oscillations. Normally it is tried to hold the mean electrical current $j_0$ in the aluminium reduction cells as constant. Therefore it is also possible to determine the basic location for the moving interface by the above described method. In this case the averaged voltage $< U >$ will be used instead of constant value $U$ in eq. (25).

### 3.2 Reconstruction of axisymmetric interface

The interface perturbation is mapped into the electrical potential in the fluid at the cylinder boundary as follows

$$\phi_k = \sum_{n=1}^{N} c_n J_0(y_n) e^{-y_n z_k} \tag{26}$$

Here $c_n$ is the amplitude of $n$-th radial mode of the interface perturbation, $\phi_k$ is the value of the electrical potential in the fluid at the cylinder wall at the $k$-th measurement point, and $z_k$ is the $z$-coordinate of the $k$-th measurement point with $1 \leq k \leq K$. The last expression can be transformed into the matrix equation

$$\phi_k = \sum_{n=1}^{N} A_{kn} c_n \tag{27}$$

where the linear operator $A_{kn} = J_0(y_n) e^{-y_n z_k}$ is also called the system matrix. A direct inversion of $A$ leading to $\eta = \phi \cdot A^{-1}$ is not in general possible for two reasons. First, the number of measurement points is usually higher than the number of modes to be reconstructed ($K > N$). In this case we would have more equations than variables. Second, the system matrix is in general ill-conditioned and the inversion of the operator $A$ becomes unstable. In this case the reconstruction error is so intense that the solution cannot be discerned from noise. We solve the presented inverse problem of the interface reconstruction in the least-square sense, i.e. we find the solution vector $\vec{\eta}$ which minimizes the deviation $\| A\vec{\eta} - \vec{\phi} \|$. A well-known technique for the solution of the linear least-squares problem is the singular value decomposition (SVD) method Press, Flannery, Teukolsky, and Vetterling (1989). Using SVD the system matrix $A$ can be written as

$$A = U \cdot diag[w] \cdot V^T \tag{28}$$

where $U$ is a $N \times K$ column-orthogonal matrix, $w$ is a

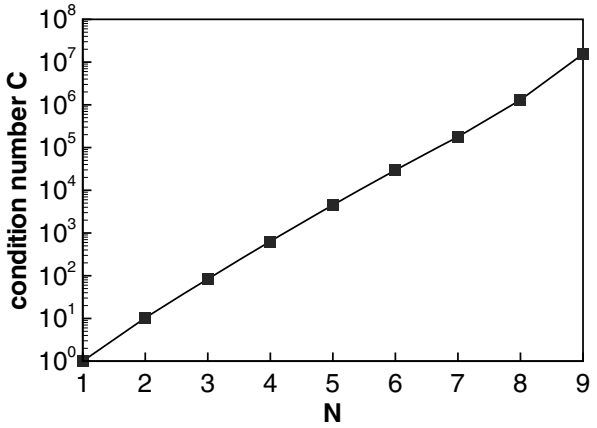


**Figure 4** : Dependence of the condition number of the system matrix on the number of the reconstructed radial modes N. The computation is performed for an axisymmetric interface and non-equidistant location of the measurement points.

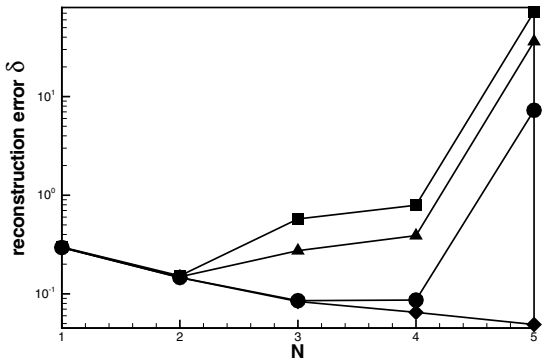


**Figure 5** : Dependence of the reconstruction error on the number of radial modes $N$ which is used for the reconstruction of the axisymmetric interface. The ♦ denote the reconstruction without data error, the • denote 1% data error, ▲ - 5% data error, ■ - 10% data error.

$K \times K$ diagonal matrix with positive elements on its diagonal only, $V$ is a $N \times N$ square orthogonal matrix. The matrices $U$ and $V$ satisfy $U^T \cdot U = V^T \cdot V = I$, where $I$ is the unitary matrix. Then the inverse operator $A^{-1}$ can be represented in the form

$$A^{-1} = V \cdot diag[w^{-1}] \cdot U^T \tag{29}$$

Based on this, we obtain the solution of the reconstruction problem as

$$\vec{\eta} = V \cdot diag[w^{-1}] \cdot (U^T \cdot \vec{\phi}) \tag{30}$$

The condition number of the system matrix $A$ is defined in the common case as $C = \| A \| \cdot \| A^{-1} \|$. If the Euclidean matrix norm is used than this is the ratio of the largest element of the matrix $w$ to the smallest element of $w$ Schwarz (1997). This number is an indicator of the difficulty of solution. The reconstructed interface at a high condition number contains a higher reconstruction error. For the present reconstruction problem it is typical that the condition number of the system matrix increases with the growth of $N$ (see Fig. 4). Thus, the more radial modes we wish to reconstruct, the higher the reconstruction error will be.

At this place it is important to comment on the choice of the number of modes to be reconstructed (number $N$ in eq. 26). Fig. 3.2 demonstrates that the reconstruction error can significantly depend on the choice of $N$, whose incorrect choice leads to non-satisfactory reconstruction results. The reconstruction error is computed as

$$\delta = \sqrt{\frac{\int_0^{2\pi}\int_0^1 [\eta(r,\varphi) - \eta_{ex}(r,\varphi)]^2 \, r\,dr\,d\varphi}{\int_0^{2\pi}\int_0^1 \eta_{ex}^2(r,\varphi) r\,dr\,d\varphi}} \tag{31}$$

where $\eta(r,\varphi)$ is the reconstructed interface, $\eta_{ex}$ is the exact interface.

To find an optimal number of modes $N$, which are used for the reconstruction, the L-curve criterion (see Hansen (1992)) is used. We solve the forward problem for a different numbers $N$ and compute for any $N$ the integral squared norm of the solution $\|\eta(r)\|$ (called solution norm below) and the squared Euclidean norm $\|A\vec{\eta} - \vec{\phi}\|$ (called residual norm):

$$\|\eta(r)\| = \int_0^{2\pi}\int_0^1 \eta^2(r) r dr d\varphi \tag{32}$$

$$\|A\vec{\eta} - \vec{\phi}\| = \sum_{k=1}^{K} \left[ (\sum_{n=1}^{N} A_{kn} \cdot c_n) - \phi_k \right]^2 \tag{33}$$

Afterwards we plot $\log \|\eta(r)\|$ as a function of $\|A\vec{\eta} - \vec{\phi}\|$. The resulting plot is typically L-shaped (Fig. 6) with a largest curvature at the optimal number of modes ($N = 2$

in most of the cases), which is the number of active modes in system. The corner of the presented curve shows the compromise between data error and reconstruction error. For small $N$ the reconstructed interface is too smooth. For $N$ greater than in the reality the data error decreases but the reconstructed interface has too large deviations, it becomes too wavy (see Fig. 7).

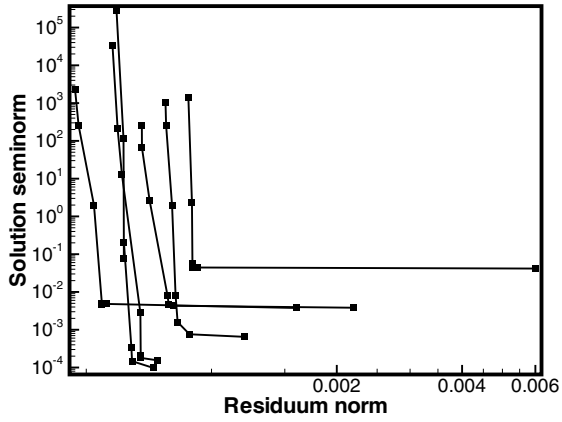


**Figure 6** : Dependence of the solution norm on the residuum norm (L-Curve) at 1% data error. The azimuthal modes with $m = 0..5$ are plotted. The optimal number of reconstructed modes is $N = 2$.

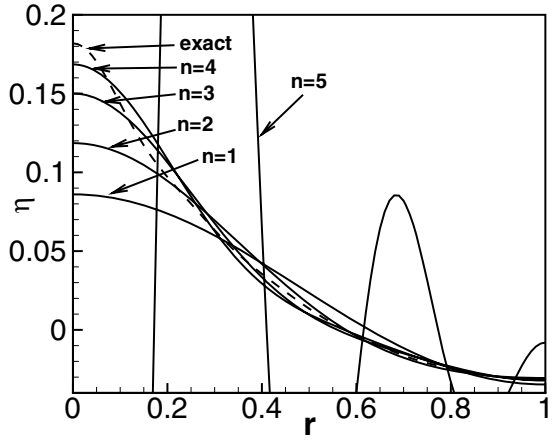


**Figure 7** : Reconstruction of axisymmetric interface with a different number of radial modes at 1% data error.

The bend of the plotted L-curve can be computed applying a method described by Kaufmann Kaufmann and Neumaier (1996). This method works as follows. Describe the vertices of L-curve as $(w_1, q_1)$, $(w_2, q_2)$, ..., $(w_l, q_l)$, where $w_1 > w_2 > \ldots > w_L$, $q_1 < q_2 < \ldots < q_L$, where $w_l$ and $q_l$ are the $l$-th values of residual norm and solution norm respectively. The regularization parameter $N$ is set for any step to $l = 1..L$. Then in the first step we compute the slopes

$$s_k = (w_{k-1} - w_k)/(q_k - q_{k-1}) \qquad k = 2,..,L \tag{34}$$

and in the second step the quotient of two consecutive slopes

$$d_k = s_k / s_{k-1} \tag{35}$$

The largest quotient $c_k$ indicates a bend of the L-curve, which is in our case the optimal number of modes to be reconstructed.

### *3.3 Reconstruction of the non-axisymmetric interface*

The mapping of the interface perturbation into the electrical potential at the fluid boundary ($r = 1$) can be described for the non-axisymmetric case as follows:

$$\phi_{kp} = \sum_{m=-M}^{M} e^{im\varphi_p} \sum_{n=1}^{N} c_{mn} J_m(y_{mn})\, e^{-y_{mn} z_k} \tag{36}$$

Here $k$ is the vertical running index of the measurement points and $p$ is the azimuthal running index. These numbers define the measurement point locations $(z_k, \varphi_p)$ respectively (see Fig. 1), and $\varphi_p = 2\pi\frac{p}{P}$, where $P$ is the number of measurement points in azimuthal direction. Eq.( 36) shows, that the reconstruction problem for the non-axisymmetric case decouples into $M$ inverse problems for the individual Fourier-modes whose mathematical structure is identical with that of the axisymmetric problem. In general, the reconstruction algorithm for the non-axisymmetric interface can be divided in two operations: 1) discrete Fourier transformation 2) solution of the inverse problem for every $m = 0..M$ with method described in the last subsection. Here $M$ is the number of azimuthal modes to be reconstructed. The diskrete Fourier transformation filters from the common data set the electrical potential which is caused by all of radial modes $n = 1...\infty$ of fixed azimuthal wave number $m$. After this we can apply the algorithm of reconstruction described above in the last subsection.

The number of azimuthal modes which we can reconstruct $M$ is limited by the number of measurement point

in azimuthal direction as $M < P/2$ according to the sampling theorem. In the practice, the good results can be achieved with a small number of $M = 1..6$. It will be discussed later in the next subsection.

The equation (36) can be transformed to

$$\phi_{kp} = \sum_{m=-M}^{M} F_{km} e^{im\varphi_p} = \sum_{m=-M}^{M} F_{km}\, e^{2\pi i m \frac{p}{P}} \tag{37}$$

where

$$F_{km} = \sum_{n=1}^{N} c_{mn} J_m(y_{mn})\, e^{-y_{mn} z_k}$$

The expression (37) presents the discretisation of a harmonic function. This function is the dependence of the electrical potential perturbation on an azimuthal angle $\phi(\varphi)$ at some fixed point on the cylinder boundary with $r = 1, z = const$.

In the first step of reconstruction a discrete Fourier transform is performed on each $k$-th row of the measurement data set $\phi_{kp}$ with $p = 0 \ldots P$, $P = 2M$ and $k = const$. This operation let us filter the electrical potential perturbations caused by the different azimuthal modes. As result the coefficients matrix $F$ is obtained as

$$F_{km} = \sum_{p=0}^{P-1} \phi_{kp}\, e^{-2\pi i \frac{p}{P}} \tag{38}$$

The m-th column $\vec{f}$ of the coefficients matrix $F$ satisfies for any $m = 1 \ldots M$ the matrix equations

$$f_k = \sum_{n=1}^{N} A_{kn} \cdot c_n \tag{39}$$

where the linear operator

$$A_{kn} = J_m(y_{mn})\, e^{-y_{mn} z_k} \tag{40}$$

is now the system matrix. The solution of such matrix equations using the singular value decomposition method has already been discussed in the subsection 3.2. The matrix $A$ can be decomposed as (30) and the particular solution for non-axisymmetric case is

$$b = V \cdot w^{-1} \cdot U^T \cdot f \tag{41}$$

Here the vector $\vec{b}$ corresponds to the $m$-th row of the amplitudes matrix $c_{mn}$. We note, that the reconstruction problem is solved for each mode with $m = 0..M$ completely independent from the other azimuthal modes.

### *3.4 Choice of optimal reconstruction parameters.*

In this subsection the choice of the number of azimuthal modes $M$, of the radial mode number $N$, and also the measurement points numbers $p$ and $k$, are discussed. The general case of non-axisymmetrical interface is discussed here, because the axisymmetric interface is a partial case of the general problem.

In the presented reconstruction problem it exist two very important parameters, namely $M$ and $N$, numbers of modes which form the reconstructed interface. In the nature it exist the infinitely number interfacial modes at the same time. As a matter we can not reconstruct all of these modes, but it is also not necessary. Really, the gravitational wave spectrum in the nature satisfies the power law Dyachenko, Korotkevich, and Zakharov (2004)

$$< |\eta_k|^2 > \sim k^{-7/2} = y^{-7/2}. \tag{42}$$

It means, that the higher modes have a very small amplitude and can be neglected without lost of important information about the interface shape to be recovered. This information can be used for the a-priori estimation of number $M$. The electrical potential perturbation $\phi$ which is produced by an azimuthal mode decline very fast with a growth of $m$ and $n$. If we consider some point on the cylinder boundary with coordinates (1,φ, z), it satisfies

$$\phi_m = sgn[z] \sum_{n=1}^{\infty} \eta(1, \varphi) \exp(-y_{mn} z).$$

The amplitudes of interfacial waves declines as shown in Eq.(42), therefore we rewrite the last expression as

$$\phi_m = sgn[z] \sum_{n=1}^{\infty} y_{mn}^{-7/4} \exp(-y_{mn} z).$$

The conclusion is that for any fixed point on the cylinder walls the higher modes produce very small electrical potential. It is smaller in comparison to the measurement error from the measurement of the strongest mode. This mode which causes the largest electrical potential on every data point is the mode with $m = 1$, $n = 1$. We have used this fact as criterion for filtering the data after Fourier decomposition procedure. In the other words, the choice of $M$, the number of azimuthal modes which are to be reconstructed, depends on the measurement error. According to this, the following numbers of azimuthal modes $M$ has been chosen in dependence on the measurement error:

**Table 1** : Dependence of $M$ on the measurement error.

| meas. error | 1% | 5% | 10% |
|---|---|---|---|
| $M$ | 6 | 3 | 3 |

The optimal number of reconstructed modes $N$ is found using the L-curve criterion, which was described above. This procedure is done for any azimuthal mode number $m = 0 \ldots M$. We have chosen $N = 2$ because the L-curves for the 6 first azimuthal modes with $m = 0..5$ have a sharp bend in the majority of cases at $N = 2$ (see Fig. 6).

After this procedure we have the numbers of modes to be reconstructed, $M$ and $N$. Then we choose the number of measurement points in the vertical direction as $k >= N$ and in azimuthal direction as $p >= 2M$. The first condition follows from the fact that the number of reconstructed modes must be smaller as the number of points in vertical direction $k$. The second one follows from the sampling theorem.

## 4 Examples of interface reconstruction

The simulation is performed in four steps as follows. First the amplitudes $c_n$ for axisymmetric or $c_{mn}$ for non-axisymmetric cases are prescribed which determine the interface shape. In the second step of the electrical potentials $\phi_k$ or ($\phi_{kp}$ in the general case) at the cylinder boundary are computed using the analytical solution (26) or (30) for the forward problem. Then in the third step random white noise is added to the obtained electrical potential data set as $\phi_{kp}(1 + \varepsilon\delta)$, where $-1 < \varepsilon < 1$ is a random number and $\delta$ is the maximum amplitude of error. These operations simulate the noisy measurement of the electrical potentials. Different noise amplitudes represent different data errors. The fourth step is the reconstruction of the interfaces employing the algorithms described in section 3.

We perform our numerical experiments for two cases. Firstly, axisymmetric interface is reconstructed and then the general case of the non-axisymmetric interface is investigated. We have try to simulate the conditions similar to the physical experiment. Therefore the amplitudes of interfacial waves are computed as

$$\eta_{mn} = y_{mn}^{-1.75} \tag{43}$$

where $y_{mn}$ is the dimensionless wavenumber for the $n$-th radial of the $m$-th azimuthal mode.

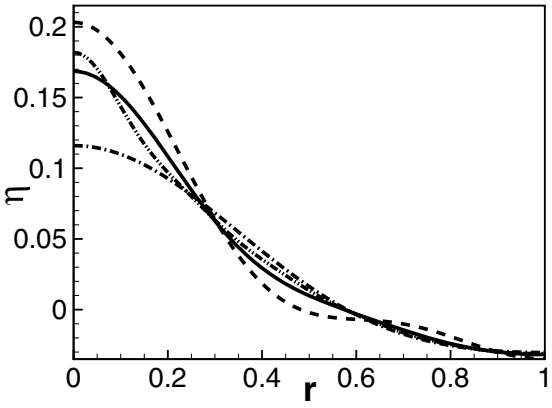


**Figure 8** : Reconstruction of the axisymmetric interface for different data errors. The exact interface is denoted with ——. The — · · — corresponds to 1% data error, the - - - - 5% data error, the — · — 10% data error.

Examples of the axisymmetric interface reconstruction are shown in Fig.8. The exact interface shape consists of the first ten modes which amplitudes are computed using Eq.(43). The number of modes $N$ which are used for the reconstruction procedure, is obtained from the L-curve (see Fig. 6). It depends on the measurement error. For 1% data error in measurement set we have used 4 modes for reconstruction, for 5% - three modes and for 10% two modes only. The reconstructed curves are very similar to the exact interface. Some deviation in the centrum of the interface ($r- > 0$) results from the fact, that the true interface has more modes in comparison to the reconstructed. However, the form of the interface is good recovered. Even if the the measurement error is high as 10%, the reconstructed interface looks similar to the exact. It demonstrates that the presented reconstruction method is robust with respect to measurement noise.

Fig. 9 presents examples of the non-axisymmetric interface reconstruction. The exact interface consists of the first ten radial modes for $m = 0, .., 10$, whose dimensionless amplitudes are computed with eq. (43). Of coarse, the reconstructed interface is smooth in comparison to the true interface consisting 100 interfacial modes because we reconstruct with a short number of interfacial modes. But the reconstructed interface is also very sim-

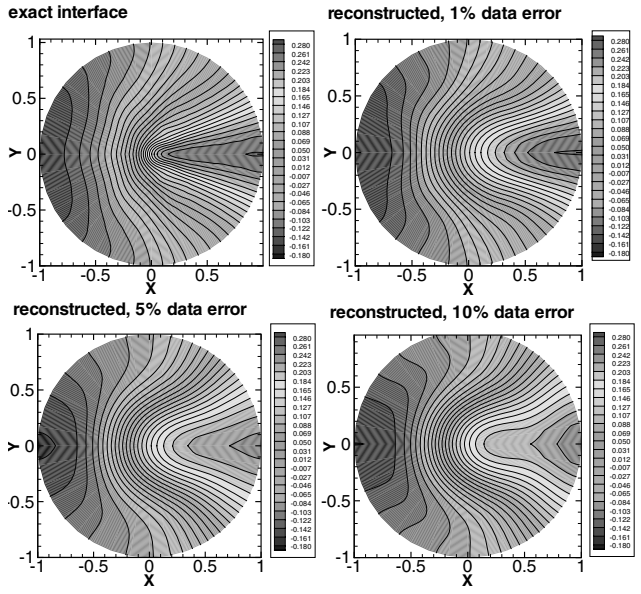


**Figure 9** : Reconstruction of the non-axisymmetric interface. View from above.

ilar with the exact interface even for the high measuring error.

## 5 Conclusion

In the present work we have described an algorithm for the interface reconstruction from electrical potential measurements at the fluid boundary in a two-fluid system with cylindrical configurations. We have investigated axisymmetric and non-axisymmetric interfaces. In both cases the interface shape is determined with good accuracy. The method is robust to measurement errors and works even at noise level as high as 10%.

Two important parameters are presented in this inverse problem. There are the numbers of modes, which are used for reconstruction, $M$ for azimuthal modes and $N$ for radial. It is shown, that $M$ can be estimated before the reconstruction. The incorrect choice of $N$ has a strong influence on the reconstruction quality and it makes the reconstruction results unacceptable. Optimal $N$ is found with the help of dependence of the integral solution norm on the residual norm, which has the typical L-curve shape and its bend corresponds to the optimal number of modes to be reconstructed. It was found the optimal $N = 2$ for the most of cases.

The presented reconstruction algorithm is based on the comparisonly simple analytical solution of the forward problem. Therefore it is much faster in comparison to the any another methods which are based on the numerical solution. The numerical cost of reconstruction is extreme low. At the other side, the reconstruction results show the good accuracy. The presented method can be used in an real-time fast interface detection system, whose application field can be the aluminium reduction cells, glass melting etc.

**Acknowledgement:** We are grateful to the Deutsche Forschungsgemeinschaft for financial support in frame of the Innovationskolleg "Magnetofluiddynamik" and to Ch Resagk, F Stefani and H Brauer for helpful discussions.

## References

**Butler, J.; Bonnecaze, R.** (1999): Imaging of particle shear migration with electrical impedance tomography. *Phys. Fluids*, vol. 11, pp. 1982–94.

**Cheney, M.; Isaacson, D.; Newell, J.** (1999): Electrical impedance tomography. *SIAM Review*, vol. 41, pp. 85–101.

**Davidson, P.** (1994): An energy analysis of unstable, aluminium reduction cells. *Eur. J. Mech., /B Fluids*, vol. 13, pp. 15–32.

**Davidson, P.** (1999): Magnetohydrodynamics in material Processing. *Annu. Rev. Fluid Mech.*, vol. 31, pp. 273–300.

**Dyachenko, A. I.; Korotkevich, A. O.; Zakharov, V. E.** (2004): Weak turbulent Kolmogorov spectrum for surface gravity waves. *Phys. Rev. Lett.*, vol. 92, no. 13.

**George, D. L.; Torczynski, J. R.; Shollenberger, K. A.; O'Hern, T. J.; Ceccio, S. L.** (2000): Validation of electrical impedance tomography for measurements of material distribution in two-phase flows. *J. Mult. Flow*, vol. 26, pp. 549–581.

**Guthrie, R. I. L.; Li, M.; Carrozza, C.** (2000): The application of the electric sensing zone to liquid metals for on-line detection of inclusion. *Proc. 3rd International Symposium on Electromagnetic Processing of Materials (Nagoya: The Iron and Steel Institute in Japan)*, pp. 31–36.

**Hansen, C.** (1992): Analysis of discrete ill-posed problems by means of the L-curve. *SIAM Review*, vol. 34, no. 4, pp. 581–613.

**Kaufmann, L. C.; Neumaier, A.** (1996): PET regularisation by envelope guided conjugate gradients. *IEEE Trans. Medical Imag.*, vol. 15, pp. 385–389.

**Miles, J.; Henderson, D.** (1990): Parametrically forced surface waves. *Annu. Rev. Fluid Mech.*, vol. 22, pp. 143–65.

**Press, W.; Flannery, B.; Teukolsky, S.; Vetterling, W.** (1989): *Numerical recipes*. Cambridge university press, Cambridge.

**Schwarz, H. R.** (1997): *Numerische Mathematik*. Teubner, Stuttgart.